Effect of continuous carbon fiber layup architecture on tensile performance of hybrid FDM composites

Evgeniy Lobov, Artem Pepeliaev, Mikhail Tashkinov
Laboratory of Mechanics of Biocompatible Materials and Devices, Perm National Research Polytechnic University, Russia
eslobov@pstu.ru, http://orcid.org/0009-0008-2855-5784
paa@pstu.ru, http://orcid.org/0009-0000-3162-2011
m.tashkinov@pstu.ru, http://orcid.org/0000-0003-4660-0020

ABSTRACT. Hybrid continuous fiber–reinforced composites produced by fused deposition modeling (FDM) offer a promising solution for lightweight load-bearing structures. However, their mechanical performance is strongly governed by internal reinforcement architecture. This study experimentally investigates the effect of continuous carbon fiber layup orientation on the tensile behavior of hybrid FDM composites based on three short-fiber-reinforced thermoplastic matrices: ABS, PA12, and PET-G. Specimens were fabricated using continuous fiber co-extrusion technology with controlled constant and combined fiber layup schemes. Uniaxial tensile tests with non-contact strain measurement were performed to evaluate Young's modulus, ultimate tensile strength, and strain-to-failure. Results show that fiber alignment with the load direction is essential for maximizing stiffness and strength, while the polymer matrix primarily controls ductility and failure strain. Combined layups with axially oriented and off-axis layers offer a balance between strength and damage tolerance. Fractographic observations indicate mixed Mode I/Mode II failure governed by structural anisotropy and matrix plasticity. These findings establish the design basics for optimizing hybrid continuous-fiber-reinforced FDM composites and provide a practical framework for the development of additively manufactured structural components.

KEYWORDS. Hybrid 3D-printed composites, Short fiber-reinforced polymers, Continuous carbon fiber, Experimental characterization, Microstructure, Layup angle.

OPEN ACCESS

Citation: Lobov E.S., Pepeliaev A.A., Tashkinov M.A., Effect of Continuous Carbon Fiber Layup Architecture on the Tensile Performance of Hybrid FDM Composites, Fracture and Structural Integrity, 77 (2026) 13-26.

Received: 29.01.2026
Accepted: 27.03.2026
Published: 03.04.2025
Issue: 07.2026

INTRODUCTION

Additive manufacturing (AM), and in particular fused deposition modeling (FDM), has rapidly evolved from a prototyping technology into a viable tool for fabricating load-bearing structural components with complex geometries and tailored internal architectures [1,2]. However, the relatively low stiffness and strength of conventional thermoplastic filaments, together with the inherent anisotropy and interlayer weakness of FDM parts, still limit their use in engineering applications requiring reliable mechanical performance. To address these limitations, two main reinforcement strategies have been widely adopted: short-fiber reinforcement and continuous-fiber reinforcement. According to the former, chopped fibers are dispersed in filaments within the polymer matrix, leading to improvements in stiffness, strength, and thermal stability while preserving printability with the same manufacturing parameters. The mechanical response of such materials strongly depends on fiber content, aspect ratio, orientation, and dispersion quality [3–8]. Despite these advantages, short fibers alone cannot provide the level of reinforcement required for highly loaded components, as load transfer is limited by fiber length and interfacial shear. A more effective approach is continuous-fiber reinforcement, implemented in FDM through continuous fiber co-extrusion (CFC) technology [9–13]. In this process, a continuous fiber tow is impregnated in situ with molten thermoplastic and deposited together with the matrix filament. This produces a composite filament during printing and enables formation of a load-bearing fibrous framework within the printed part. Continuous fibers carry the majority of the applied load, while the thermoplastic matrix ensures stress transfer, geometric integrity, and interlayer bonding. The ability to control the spatial arrangement of reinforcement during printing represents a fundamental advantage of additive manufacturing over conventional composite processing. In FDM, fiber orientation, stacking sequence, and local reinforcement density can be varied within a single component, enabling the creation of architected composite structures with region-specific mechanical responses. Such controlled reinforcement allows to align fibers with principal stress directions, redistribute loads, mitigate stress concentrations, and tailor stiffness and strength. This design freedom is essential for moving from uniform, isotropic parts toward functionally graded, application-specific composite architectures.

In recent years, hybrid reinforcement systems combining a short-fiber-reinforced polymer matrix with embedded continuous fibers have also attracted increasing attention [14–18]. In such materials, the short fibers enhance the stiffness and strength of the matrix and improve load transfer to the continuous reinforcement, while the continuous fibers provide a structural framework that carries the primary load. The performance of such FDM composites is highly sensitive to the internal reinforcement architecture. In particular, the orientation of continuous fibers relative to the applied load governs load-transfer efficiency, the development of interlaminar shear, and the dominant failure mechanisms [19]. Off-axis fiber orientations introduce shear-dominated stress states, reduce the axial load-bearing capacity of the fibers, and increase the role of the polymer matrix and the fiber–matrix interface. Consequently, the mechanical properties can vary by several times depending on the selected layup configuration, even for the same material system and fiber content.

However, while the importance of fiber alignment is widely acknowledged, quantitative relationships between layup angle, reinforcement architecture (single vs. combined), and failure mechanisms remain poorly established for hybrid FDM composites produced by continuous fiber co-extrusion. Continuous-fiber FDM is typically studied in isolation, often using only nylon- or PLA-based matrices and a small number of fiber orientations [12,13,20]. Existing works on hybrid systems combining short-fiber matrices and continuous fibers generally lack a controlled comparison of layup schemes [21,22]. Thus, systematic experimental data on the effect of continuous fiber layup angle in hybrid FDM composites with different polymer matrices remain limited.

The present work addresses this gap by experimentally investigating the influence of continuous carbon fiber (CCF) layup angle on the tensile mechanical response of hybrid FDM composites based on three widely used thermoplastics: acrylonitrile–butadiene–styrene (ABS), polyamide-12 (PA12), and polyethylene-terephthalate-glycol (PET-G), each reinforced with short fibers. These polymers were selected due to their widespread use in additive manufacturing and their distinct mechanical and physical characteristics. ABS is known for its relatively high strength and impact resistance, PA12 exhibits high ductility and chemical stability, and PET-G provides an intermediate combination of strength, flexibility, and processability. Specimens were manufactured using continuous fiber co-extrusion technology using various constant and combined fiber layup schemes and tested under uniaxial tension. The dependences between reinforcement architecture, stiffness, strength, and failure behavior were analyzed, providing design guidelines for optimizing load-bearing hybrid FDM composites for engineering applications.

MATERIALS AND METHODS

Materials and additive manufacturing

To enhance the mechanical performance of the matrix, each studied polymer was reinforced with short fibers: carbon fibers (CF) for ABS and PA12, and glass fibers (GF) for PET-G. The resulting composite filaments were denoted as ABS+CF (density 1.11 g/cm³), PA12+CF (1.06 g/cm³), and PET-G+GF (1.23 g/cm³). These short-fiber-reinforced polymers served as the matrix material for all specimens.

CCF filament supplied by Anisoprint (Shanghai, China) was used as the primary load-bearing reinforcement. The CCF consisted of 1.5K carbon fibers with a nominal Young's modulus of 149 GPa and an ultimate tensile strength of 2206 MPa. The fiber bundle was pre-impregnated with a thermoset sizing and had a nominal diameter of 350 μm, corresponding to a fiber volume fraction of approximately 60%.

All specimens were fabricated using an Anisoprint Composer A4 dual-extrusion 3D printer (Anisoprint, Shanghai, China) equipped with a standard thermoplastic nozzle (0.4 mm diameter) and a continuous fiber co-extrusion nozzle (0.6 mm diameter). The CFC process feeds both the CCF filament and the molten thermoplastic into the same print head, where the polymer coats the fiber bundle immediately prior to deposition. This *in-situ* impregnation promotes interfacial adhesion between the continuous fibers and the thermoplastic matrix, enabling the formation of a load-bearing composite architecture during printing. The scheme of the printing process is illustrated in Fig. 1.

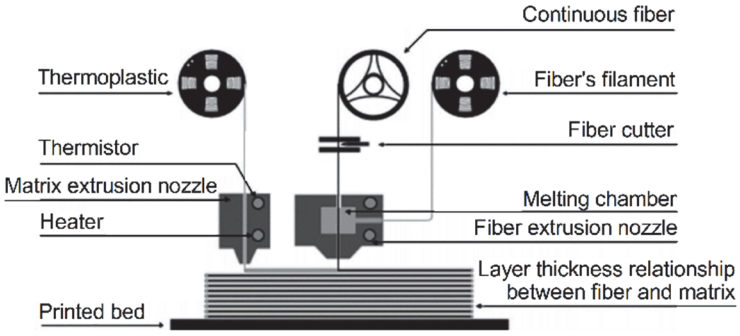

Figure 1: Printing process scheme for CFC technologies.

The printing parameters for the three matrix materials are summarized in Tab. 1. The build platform temperature, nozzle temperature, and printing speed were optimized for each polymer to ensure stable extrusion, good interlayer bonding, and effective fiber impregnation. The thermoplastic matrix was deposited at a printing speed of 50 mm/s, while the continuous fiber was placed at 10 mm/s to ensure accurate fiber placement and proper wetting by the molten polymer. The first layer was printed with a thickness of 0.26 mm, followed by layers of 0.29 mm thickness.

		Extruder #1			Extruder #2
		ABS+CF	PA12+CF	PET-G+GF	CCF
Nozzle diameter, mm		0.4			0.6
Layer height, mm	Layer #1	0.26			
	Layers #2-7	0.29			
Print platform temperature, °C		100	60	90	-
Nozzle temperature, °C		250	265	250	-
Printing speed, mm/sec		50			10

Table 1: Manufacturing parameters for continuous fiber-reinforced specimens.

Geometry and configuration of CCF-reinforced samples

To investigate the influence of CCF layup angle and reinforcement scheme on the tensile behavior of hybrid FDM composites, rectangular prismatic specimens were designed and manufactured (Fig. 2). The geometry was selected to ensure a uniform stress state in the gauge section and to allow controlled variation of fiber orientation within the printed layers. All specimens were printed with a fixed total number of layers, while continuous fiber reinforcement was introduced only in the three central layers (layers 3–5). This configuration ensured symmetric reinforcement through the specimen thickness

and minimized bending effects during tensile loading. The remaining layers consisted of short-fiber-reinforced thermoplastic only.

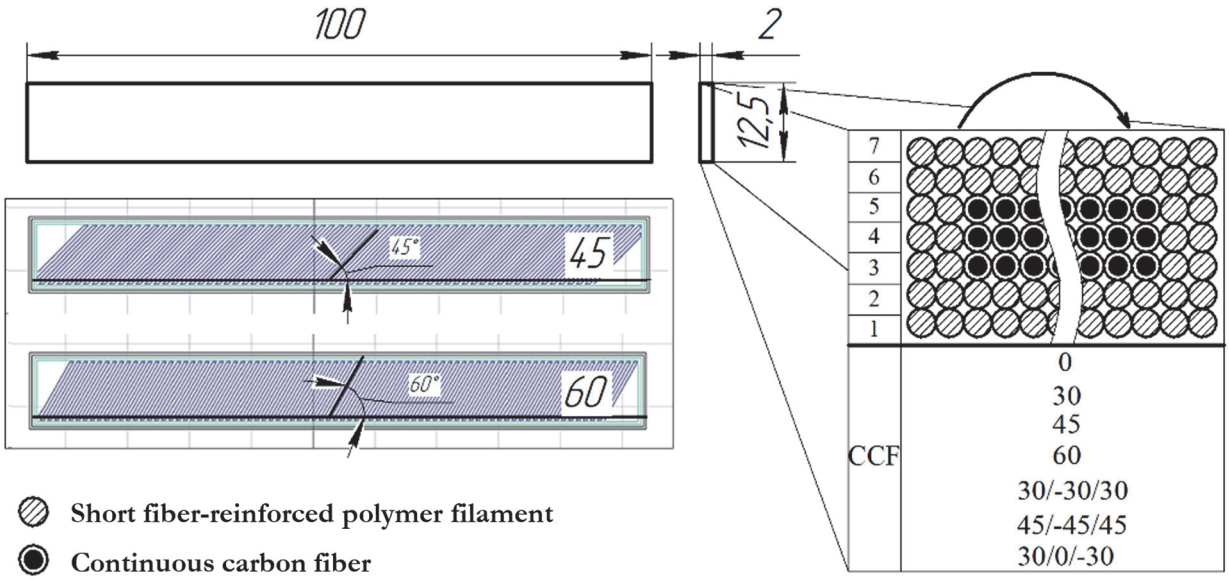

Figure 2: Geometry of CCF-reinforced samples.

Within the reinforced region, the CCF was deposited at prescribed angles relative to the tensile loading direction. Constant layup angles of 0°, 30°, 45°, and 60° were investigated, representing fiber orientations from fully aligned with the load (0°) to highly off-axis (60°). In addition, three combined layup schemes were studied to simulate quasi-laminate architectures: 30°/0°/−30°, 30°/−30°/30°, and 45°/−45°/45°, where the sequence denotes the fiber orientation in the third, fourth, and fifth layers, respectively. For clarity, the notation "PA12+CF+CCF 30" refers to a specimen printed from a PA12+CF matrix with continuous carbon fibers oriented at 30° in each of the three reinforced layers. Similarly, "PA12+CF+CCF 45/−45/45" denotes a specimen in which the CCF was placed at 45° in the third layer, −45° in the fourth layer, and 45° in the fifth layer.

The continuous fibers were aligned within each layer along straight paths corresponding to the prescribed angles, while the thermoplastic matrix was deposited in parallel raster lines oriented along the tensile loading direction. This approach ensured a consistent matrix architecture for all specimens, allowing the effects of continuous fiber orientation to be isolated. Such sample design enabled a systematic evaluation of how both constant and combined CCF layup schemes influence stiffness, strength, and failure behavior under uniaxial tensile loading.

Experimental tests

Uniaxial tensile tests were performed at room temperature (approximately 20°C) using an Instron 68SC-5 universal testing machine (Instron, Norwood, MA, USA) equipped with a 5 kN load cell. The tests were conducted under displacement control at a constant crosshead speed of 1 mm/min. Strain was measured using a non-contact AVE2 video extensometer (Instron, Norwood, MA, USA). Two reference markers were applied to the surface of each specimen at equal distances from the center of the gauge section and aligned with the loading direction. The relative displacement between these markers was continuously tracked during loading, allowing direct measurement of axial strain (Fig. 3). The testing of specimens made from ABS+CF+CCF 0°, PA12+CF+CCF 0°, and PET-G+GF+CCF 0° was carried out using a universal testing machine Instron 3369 with a maximum load capacity of 50 kN. The mechanical tests were performed under the same experimental parameters as in the previous test series.

For each material and layup configuration, at least nine specimens were tested to ensure statistical reliability and to assess repeatability. Force–displacement data were recorded continuously and converted to engineering stress–strain curves employing the initial cross-sectional area and length of each specimen. The Young's modulus was determined from the initial linear region of the stress–strain curve, while the ultimate tensile strength and strain at break were taken as the maximum stress and corresponding strain prior to failure. All reported values represent the mean and standard deviation of the test series.

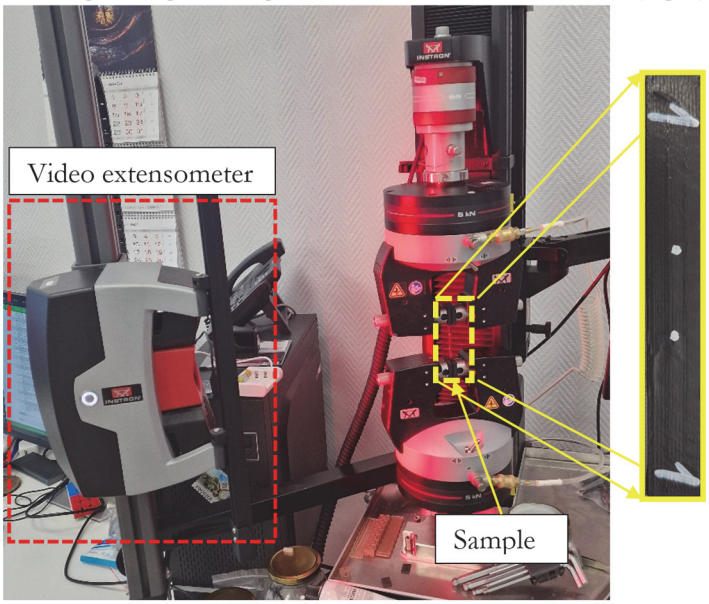

Figure 3: Tensile experiment setup with a video extensometer and a specimen with control markers.

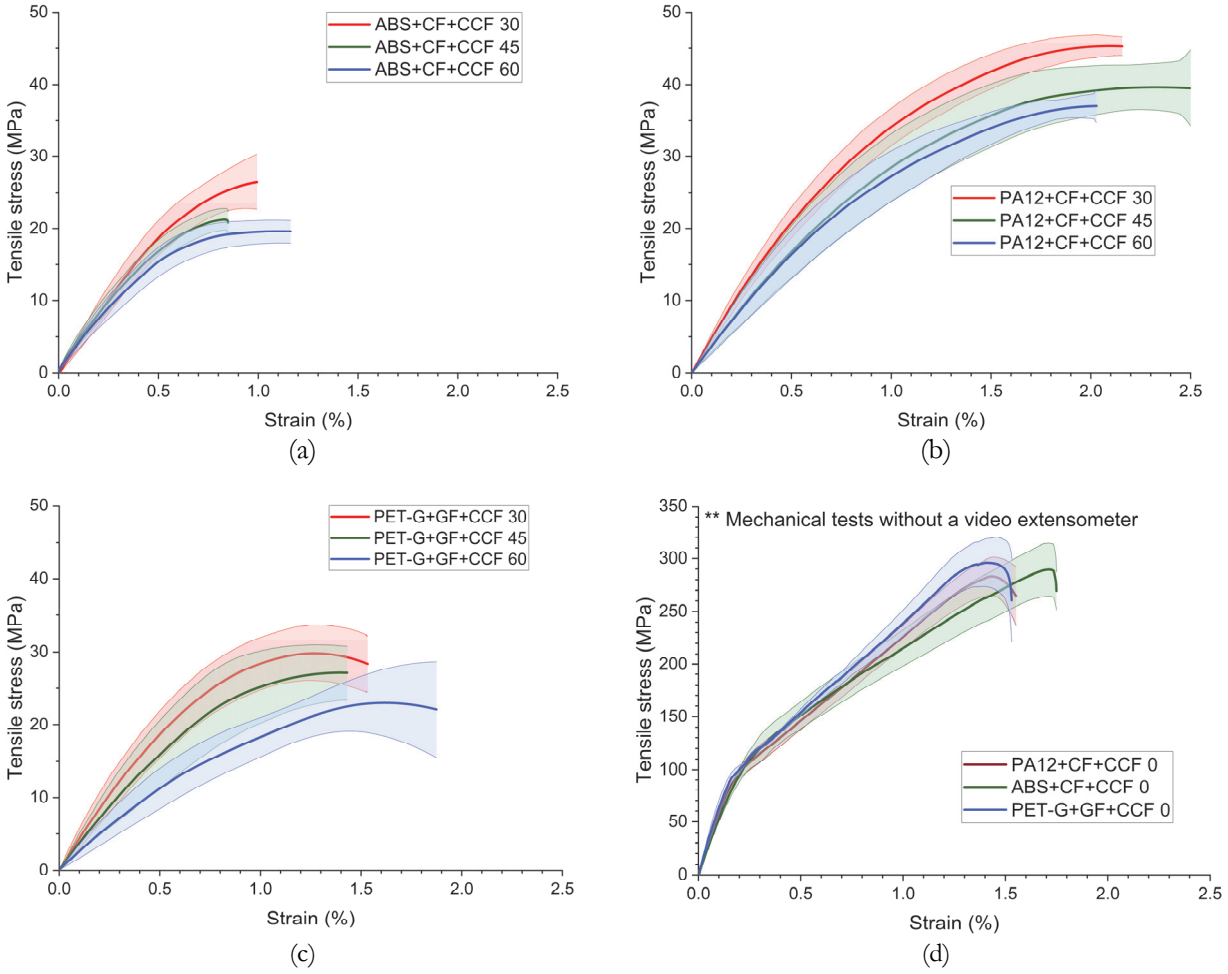

Figure 4: Stress-strain curves for samples reinforced with CCFs at a constant layup angle: (a) ABS+CF+CCF, (b) PA12+CF+CCF, (c) PET-G+GF+CCF, (d) All materials with a CCF layup angle 0°.

RESULTS

The tensile response of the studied hybrid composites showed a strong dependence on both the CCF layup angle and the reinforcement scheme. For all three matrix systems (ABS+CF, PA12+CF, and PET-G+GF), systematic variations in stiffness, ultimate tensile strength, and failure strain were observed. Fig. 4 presents stress–strain curves for hybrid composites reinforced with CCFs at constant layup angles of 30°, 45°, and 60° for (a) ABS+CF+CCF, (b) PA12+CF+CCF, and (c) PET-G+GF+CCF. The corresponding curves for specimens with fibers aligned with the loading direction (0°) are shown separately in Fig. 4d in order to preserve the scale.

For all three materials, the stress–strain response was strongly governed by fiber orientation. The 30° layup consistently exhibited the highest stiffness and strength among the off-axis configurations. As the layup angle increased from 30° to 60°, a systematic reduction in both the initial slope and the ultimate stress was observed, reflecting the progressive loss of axial load-bearing efficiency of the continuous fibers.

A comparison between the three material systems revealed some differences in mechanical performance and deformation behavior. For the same layup angle, PA12+CF+CCF generally exhibited the highest strength and strain-to-failure values, indicating more effective stress redistribution and greater ductility of the PA12-based matrix. PET-G+GF+CCF showed intermediate behavior, with moderate stiffness and strength but higher ductility than ABS-based composites. In contrast, ABS+CF+CCF displayed the lowest ultimate strain and the most brittle response, characterized by a steeper elastic region and abrupt failure. These differences were most evident at higher layup angles (45° and 60°), where the deformation mechanism became increasingly matrix-dominated. Under these conditions, the superior ductility of PA12 allows it to sustain higher strains before failure, while the lower toughness of ABS leads to earlier fracture. PET-G exhibited transitional behavior between these two.

In the case of the 0° layup (Fig. 4d), the stress–strain curves for all three materials were nearly coincident, indicating that when fibers are aligned with the loading direction, the composite response is controlled primarily by the CCFs rather than the polymer matrix: the fibrous framework dominates load transfer under axial loading, while the matrix plays a secondary role in maintaining structural integrity and stress transfer.

Fig. 5 presents bar charts of Young's modulus, ultimate tensile strength, and strain at failure for hybrid composites as a function of the CCF layup angle for the three matrix systems. The numerical data obtained are summarized in Tab. 2.

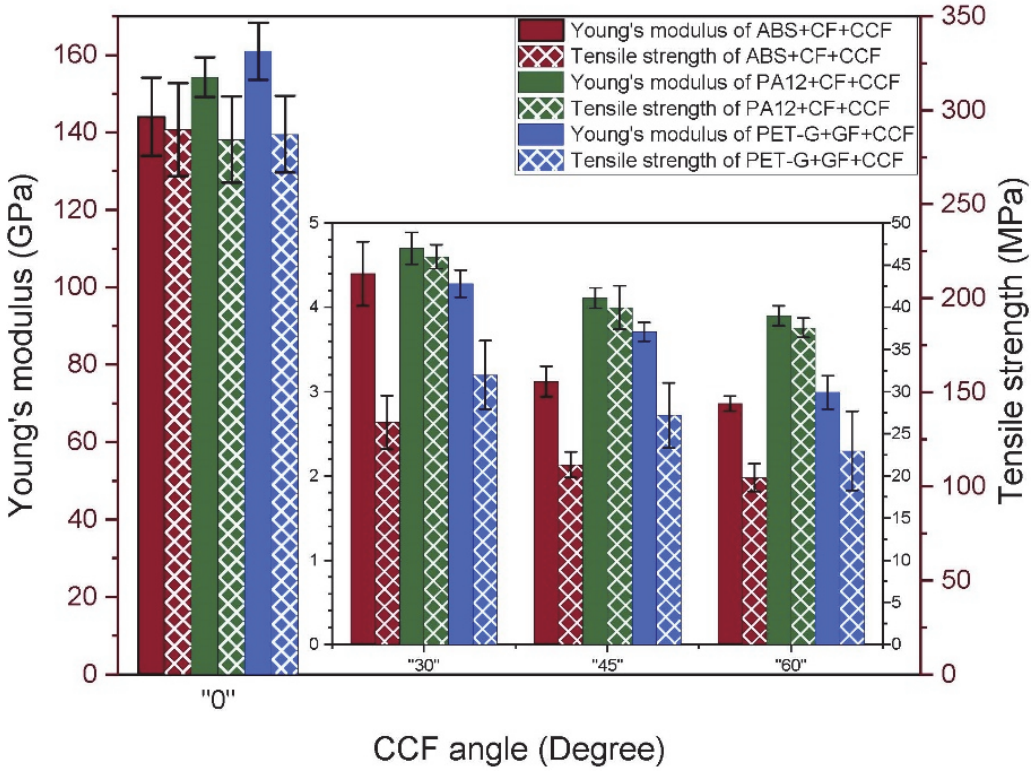

Figure 5: Tensile mechanical properties of materials as a function of the layup angle of CCF.

For specimens with constant angle layers (30°, 45°, and 60°), both Young's modulus and ultimate tensile strength decreased monotonically with increasing deviation of reinforcement from the loading axis, as seen in the stress–strain curves in Fig. 4 and the bar charts in Fig. 5. For the ABS+CF+CCF samples, increasing the fiber angle from 30° to 60° reduced Young's modulus from 4.40 to 2.86 GPa and the ultimate tensile strength from 26.35 to 19.80 MPa. For PA12+CF+CCF, the modulus decreased from 4.70 to 3.90 GPa and the strength from 46.00 to 37.58 MPa. A more pronounced sensitivity to orientation was observed for PET-G+GF+CCF, where the modulus decreased from 4.28 to 2.99 GPa and the strength from 31.99 to 22.96 MPa. These reductions reflect the transition from fiber-dominated axial loading to matrix- and interface-dominated shear loading. As the fiber orientation rotated away from the load direction, the axial stress component carried by the fibers diminished, while interlaminar shear and matrix deformation increasingly govern the mechanical response.
A comparison between materials reveals that PA12+CF+CCF exhibited the highest ultimate tensile strength at all investigated angles, followed by PET-G+GF+CCF, while ABS+CF+CCF consistently showed the lowest strength. In contrast, differences in Young's modulus among the three systems were less pronounced, indicating that stiffness is primarily governed by the continuous fiber framework, whereas strength and failure strain are more sensitive to the matrix properties. Stress–strain curves for combined layup configurations are presented in Fig. 6.

Material	Young's module, GPa	Ultimate stress, MPa	Ultimate strain, %
ABS+CF+CCF 0 deg	47.78±2.02	265.14±24.08	1.75±0.07
ABS+CF+CCF 30 deg	4.40±0.38	26.35±3.16	0.99±0.18
ABS+CF+CCF 45 deg	3.12±0.18	21.32±1.52	0.85±0.13
ABS+CF+CCF 60 deg	2.86±0.09	19.80±1.66	1.16±0.28
PA12+CF+CCF 0 deg	61.72±0.99	283.84±22.31	1.55±0.15
PA12+CF+CCF 30 deg	4.70±0.19	46.00±1.42	2.26±0.31
PA12+CF+CCF 45 deg	4.11±0.12	39.99±2.58	2.54±0.73
PA12+CF+CCF 60 deg	3.90±0.12	37.58±1.14	2.03±0.68
PET-G+GF+CCF 0 deg	66.97±1.08	296.15±20.77	1.53±0.17
PET-G+GF+CCF 30 deg	4.28±0.16	31.99±4.07	1.51±0.20
PET-G+GF+CCF 45 deg	3.71±0.11	27.18±3.88	1.43±0.45
PET-G+GF+CCF 60 deg	2.99±0.20	22.96±4.69	1.87±0.43

Table 2: Test results for continuous fiber-reinforced materials.

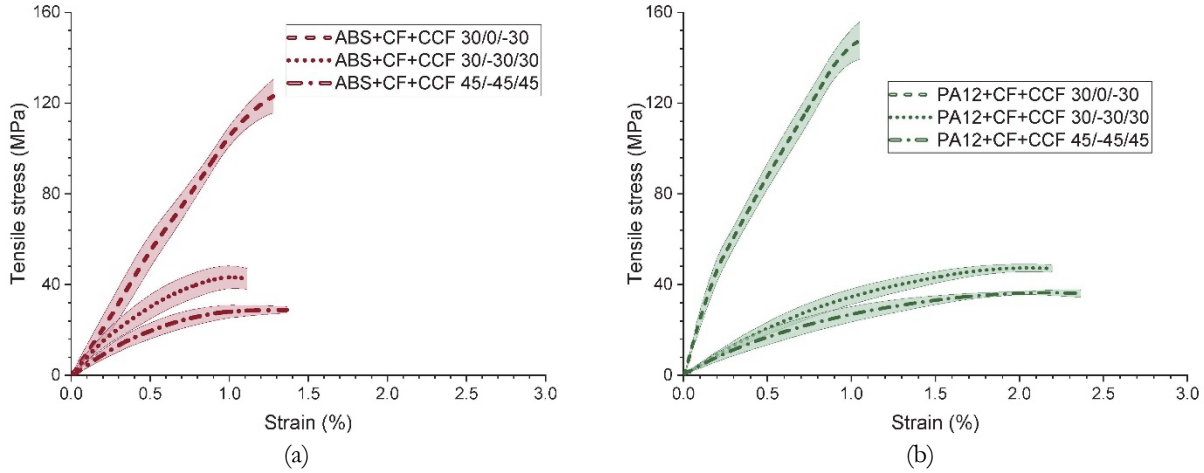

(a) (b)

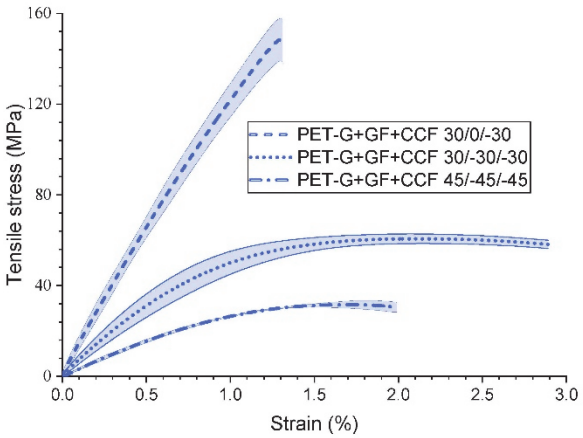

(c)

Figure 6: Stress-strain curves for samples reinforced by CCF with combined layup: (a) ABS+CF+CCF, (b) PA12+CF+CCF, (c) PET-G+GF+CCF.

For all three matrices, the 30/0/−30 configuration exhibited the steepest initial slope and the highest peak stress, indicating the greatest stiffness and strength. The stress–strain curves for this layup were shifted upward relative to the other two combinations. This reflects the presence of a direct axial load path via the 0° layer: continuous fibers aligned with the loading direction carry the majority of the tensile load, while the ±30° layers provide additional constraint and redistribution of shear stresses. The high peak stress and comparatively limited nonlinearity before failure were consistent with fiber-dominated response. Without the 0° layer, the curves showed a pronounced reduction in both slope and peak stress for each material. Between the two off-axis layup schemes, 30/−30/30 consistently outperformed 45/−45/45, evidenced by higher initial stiffness and higher ultimate stress. This ordering indicates that as the average fiber orientation deviates further from the loading axis (moving from ±30° to ±45°), the composite response becomes increasingly governed by matrix deformation, fiber–matrix interfacial shear, and interlayer shear, which limits load transfer to the fibers and reduces strength. Comparing materials with the same layup scheme, the curves showed systematic differences in deformation behavior. ABS+CF+CCF (Fig. 6a) exhibited relatively abrupt failure and the lowest terminal strain, indicating lower toughness and a reduced ability of the ABS-based matrix to accommodate shear-dominated damage. PET-G+GF+CCF (Fig. 6c) showed more pronounced nonlinearity and higher strain levels prior to failure, particularly for the off-axis layups, which suggests a greater capacity for plastic deformation and stress redistribution in the PET-G-based matrix. PA12+CF+CCF (Fig. 6b) demonstrated an intermediate response consistent with a mixed failure character, where both matrix plasticity and more brittle mechanisms are involved.

Bar charts of Young's modulus, ultimate tensile strength, and strain at failure for hybrid composites as a function of the CCFs layup scheme are presented in Fig. 7. The quantitative values are listed in Tab. 3.

For ABS+CF+CCF, the 30/0/−30 layup reached an ultimate tensile strength of 123.04 MPa and a Young's modulus of 7.33 GPa, representing a 4.7-fold increase in strength compared with the 30° constant-angle layup and a more than sixfold increase relative to the 60° configuration. For PA12+CF+CCF, the corresponding values were 148.32 MPa and 7.35 GPa, while for PET-G+GF+CCF they reached 151.27 MPa and 8.10 GPa.

In contrast, the combined layups that did not include an axially oriented layer showed lower performance. The 30/−30/30 configuration resulted in reductions of stiffness and strength of approximately 28% and 64%, respectively, relative to the 30/0/−30 case. The 45/−45/45 scheme exhibited even more severe degradation, with stiffness and strength decreases exceeding 49% and 77%, respectively. This trend was consistent across all three matrix systems. The sequence 30/0/−30 > 30/−30/30 > 45/−45/45 in terms of both stiffness and strength was consistently observed for ABS+CF, PA12+CF, and PET-G+GF composites.

Unlike stiffness and strength, the ultimate strain showed a stronger dependence on the matrix material rather than on the fiber architecture alone. The highest strain in the entire dataset was observed for PET-G+GF+CCF 30/−30/30 (2.89%), followed by PA12+CF+CCF 45/−45/45 (2.37%). In contrast, ABS+CF+CCF specimens exhibited consistently lower strain values, reflecting the more brittle nature. For configurations containing a 0° layer, such as 30/0/−30, the strain at failure was reduced compared with off-axis-dominated layups, indicating a transition to fiber-controlled, less ductile failure mechanisms.

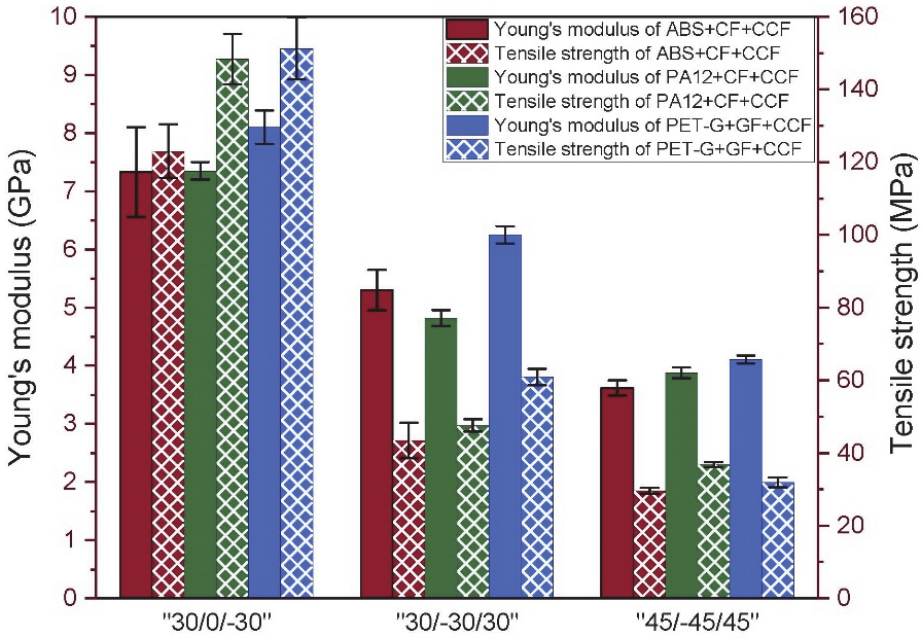

Figure 7: Tensile mechanical properties of samples with quasi-laminate architecture as a function of the reinforcement scheme.

Material	Young's module, GPa	Ultimate stress, MPa	Ultimate strain, %
ABS+CF+CCF 30/0/-30	7.33±0.77	123.04±7.40	1.28±0.32
ABS+CF+CCF 30/-30/30	5.30±0.35	43.46±4.83	1.11±0.30
ABS+CF+CCF 45/-45/45	3.62±0.13	29.57±0.79	1.50±0.30
PA12+CF+CCF 30/0/-30	7.35±0.15	148.32±6.98	1.05±0.08
PA12+CF+CCF 30/-30/30	4.82±0.14	47.62±1.68	2.20±0.26
PA12+CF+CCF 45/-45/45	3.88±0.09	36.86±0.72	2.37±0.98
PET-G+GF+CCF 30/0/-30	8.10±0.29	151.27±8.51	1.32±0.09
PET-G+GF+CCF 30/-30/30	6.25±0.15	60.92±2.19	2.89±0.67
PET-G+GF+CCF 45/-45/45	4.11±0.07	31.93±1.35	1.99±0.14

Table 3: Test Results for Continuous Fiber-Reinforced Materials.

Discussion

The experimental results demonstrated that the mechanical response of hybrid FDM composites reinforced with continuous carbon fibers (CCF) is governed primarily by the orientation of the fibrous framework relative to the loading direction. Across all matrix systems studied (ABS+CF, PA12+CF, and PET-G+GF), a systematic reduction in stiffness and strength was observed as the CCF layup angle deviated from the tensile axis. This behavior is consistent with classical laminated composite mechanics, in which the axial load-bearing contribution of the fibers decreases with increasing off-axis orientation, while the role of matrix deformation and interlaminar shear progressively increases. For comparison, the short-fiber reinforced matrices used in this work (ABS+CF, PA12+CF and PET-G+GF) without continuous carbon fiber reinforcement exhibit Young's modulus values typically in the range of 2–3 GPa and tensile strengths of 30–60 MPa, as reported in our previous study [4]. This confirms that the substantial increase in stiffness and strength observed for the 0° configuration is associated with the load-bearing contribution of the continuous carbon fibers. The large difference between the mechanical properties of the 0° configuration and off-axis layups should also be considered in relation to the internal reinforcement architecture. Continuous carbon fibers were introduced only in three central layers

and therefore form a discrete load-bearing framework rather than a classical laminated composite. When fibers are aligned with the loading direction, the applied load was transferred directly along the high-modulus carbon fibers, leading to stiffness values exceeding 40–60 GPa.

When fibers were oriented away from the loading axis, the axial stress component carried by the fibers decreases and the mechanical response becomes governed by matrix deformation and fiber-matrix interfacial shear. This transition explains the monotonic degradation of Young's modulus and ultimate tensile strength from 30° to 60° observed for all materials, as well as the enhanced sensitivity to processing-induced defects and interlayer bonding quality at higher angles. Such reinforcement architectures are nevertheless important in practical composite design, where off-axis layers improve shear resistance, crack deflection capability, and structural stability under multi-axial loading conditions. Therefore, off-axis CCF layers should be considered as structural elements that complement axial reinforcement rather than as independent load-bearing components.

When the reinforcement architecture included a 0° layer, the mechanical response changes fundamentally. The combined layup scheme of 30/0/−30 provided a continuous axial load path through the specimen thickness and therefore maximized both stiffness and strength for all matrix systems. This effect was evident in the substantial increase in mechanical performance relative to single-angle or off-axis-only schemes. The presence of the 0° layer ensured that a significant fraction of the applied load was directly borne by the continuous fibers, while the surrounding off-axis layers served to redistribute shear stresses and reduce stress concentrations, stabilizing the composite structure. Combined layups without a 0° layer component, such as 30/−30/30 and 45/−45/45, exhibited a pronounced loss of stiffness and strength.

The strain-to-failure behavior revealed a complementary role of the polymer matrix. This was particularly evident in the PA12+CF and PET-G+GF systems, which exhibited significantly higher strain values compared with ABS-based composites for off-axis and combined layups. The observed differences may reflect the intrinsic viscoelastic–plastic properties of the matrices and their ability to accommodate local stress concentrations through plastic deformation.

The fracture morphologies shown in Figs. 8 and 9 provide further insight into the underlying failure mechanisms. The red lines on the images in Fig. 8 play role of geometric benchmarks for evaluating the fracture trajectory in tested specimens. The oblique red line approximates the orientation of the principal crack, while the vertical red line establishes a reference aligned precisely with the direction of applied load. The results confirm that failure trajectory was governed by the combined effects of loading angle, structural anisotropy, and material plastic deformation capacity. In all cases, a mixed (Mode I + Mode II) failure mechanism was noted, while increase of the loading angle partially stabilized the crack trajectory.

For constant-angle specimens (Fig. 8), the crack trajectory deviated from the loading direction and followed a path dictated by the anisotropic reinforcement architecture. ABS-based composites displayed stepwise, quasi-brittle fracture with a narrow plastic zone, whereas PA12-based composites showed more stable crack growth with a pronounced plastic deformation region. PET-G-based composites exhibited intermediate behavior, characterized by mixed brittle–ductile features.

For combined layups (Fig. 9), the crack paths also deviated significantly from the nominal loading direction, highlighting the strong influence of internal architecture on fracture evolution. The presence of off-axis layers promoted a mixed Mode I/Mode II failure mechanism, in which shear-driven crack deflection partially stabilized crack propagation but did not compensate for the loss of axial load-bearing capacity. These observations confirm that structural anisotropy, fiber orientation, and matrix plasticity jointly control the failure response of hybrid FDM composites.

a) 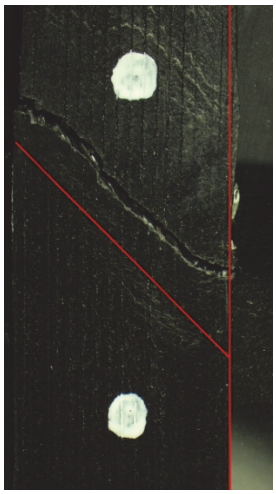 b)  c) 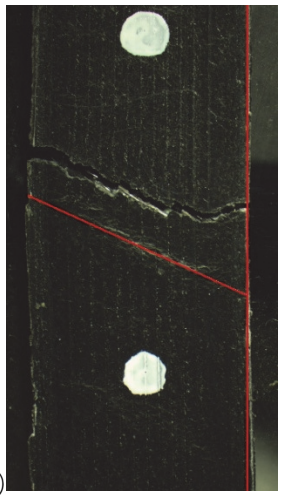

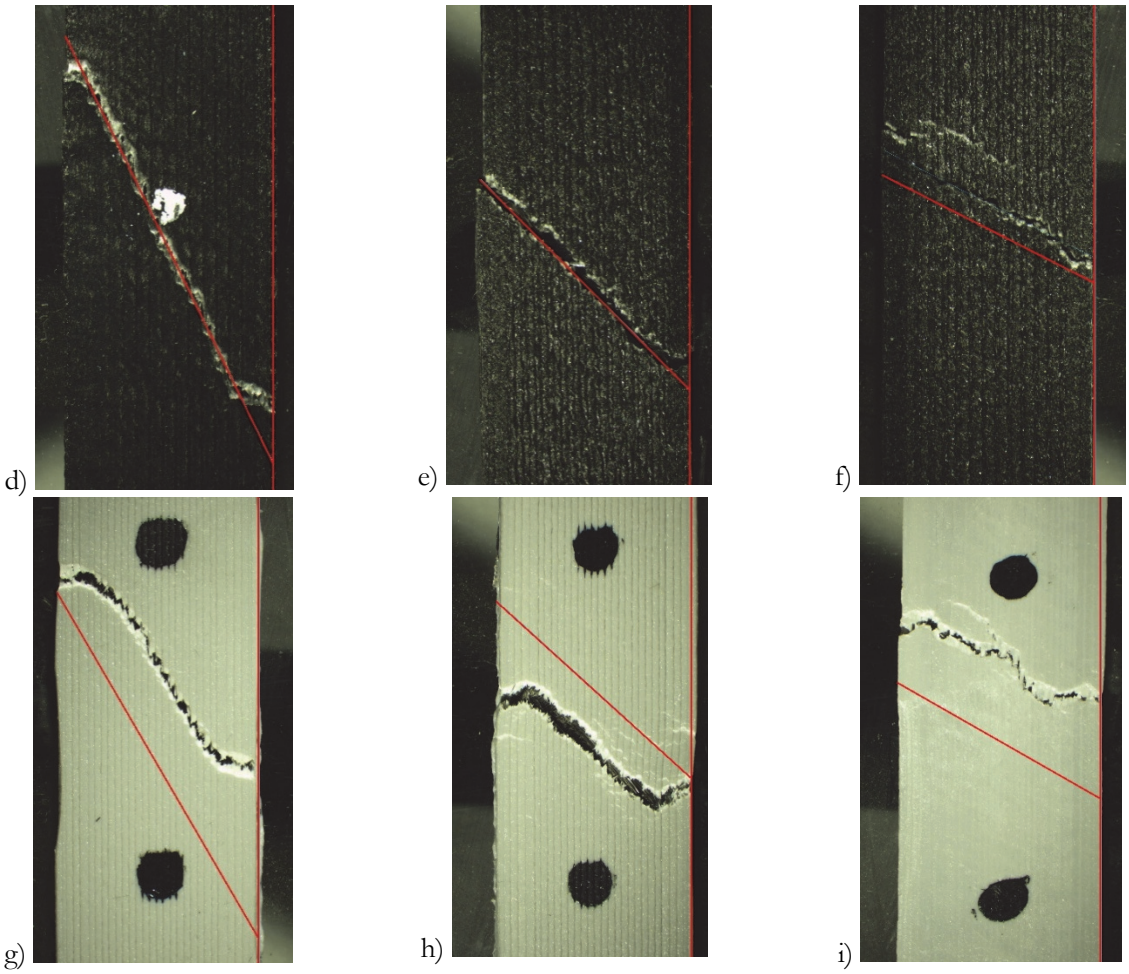

Figure 8: Morphology of fractured samples: (a) ABS+CCF 30, (b) ABS+CCF 45, (c) ABS+CCF 60, (d) PA12+CCF 30, (e) PA12+CCF 45, (f) PA12+CCF 60, (g) PET-G +CCF 30, (h) PET-G +CCF 45, (i) PET-G +CCF 60.

From an engineering perspective, the results allow to establish a design principle: for components subjected predominantly to uniaxial or bending loads, reinforcement architectures must include fiber layers aligned with the principal load direction. Off-axis layers should be used strategically to improve damage tolerance and shear resistance. At higher layup angles, the role of process quality, such as fiber impregnation, interfacial adhesion, and interlayer bonding, becomes increasingly critical, as the composite response transitions from fiber-dominated to matrix- and interface-controlled.

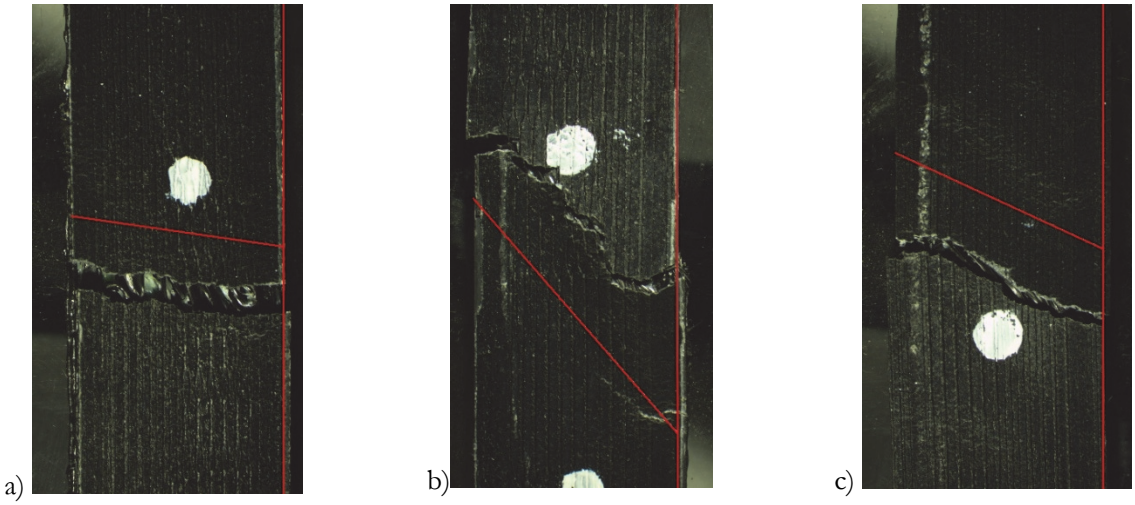

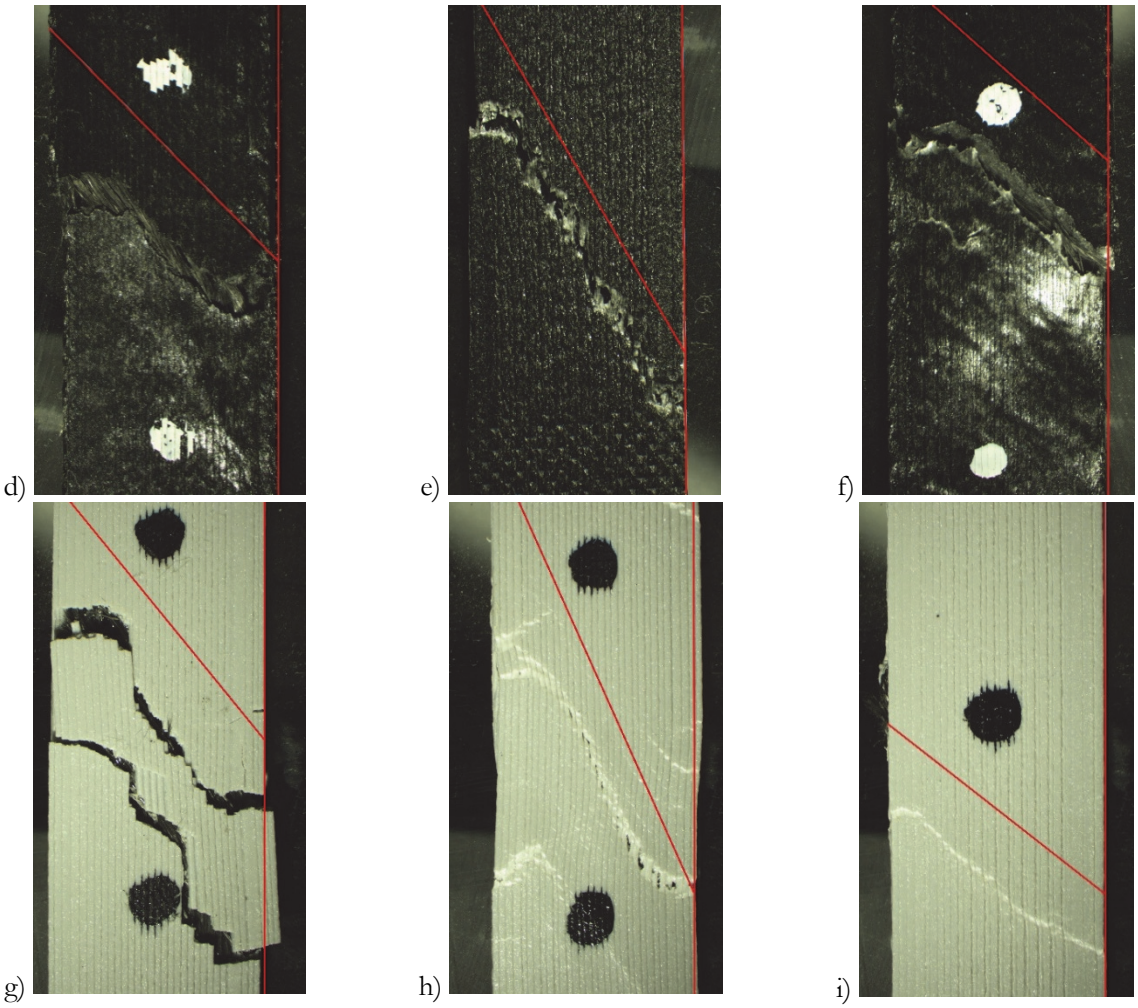

Figure 9: Morphology of fractured samples: (a) ABS+CCF 30/0/-30, (b) ABS+CCF 30/-30/30, (c) ABS+CCF 45/-45/45, (d) PA12+CCF 30/0/-30, (e) PA12+CCF 30/-30/30, (f) PA12+CCF 45/-45/45, (g) PET-G +CCF 30/0/-30, (h) PET-G +CCF 30/-30/30, (i) PET-G+CCF 45/-45/45.

Conclusions

This study investigated the influence of continuous carbon fiber layup architecture on the tensile mechanical response of hybrid FDM composites based on short-fiber-reinforced ABS, PA12, and PET-G matrices. It was demonstrated that both stiffness and ultimate tensile strength decrease systematically as the fiber layup angle deviates from the loading direction, confirming that the axial projection of the continuous fibers controls the efficiency of load transfer. Reinforcement schemes that include a 0°-oriented layer provide a continuous axial load path and therefore achieve the highest strength and stiffness, with the 30/0/−30 configuration consistently outperforming all other layups. While the continuous fibers dominate stiffness and strength, the polymer matrix primarily governs ductility and failure strain, with PA12-based composites showing the highest elongation, PET-G-based systems intermediate behavior, and ABS-based composites the most brittle response. Fracture observations further reveal that crack trajectories are strongly influenced by structural anisotropy and matrix plasticity, resulting in mixed Mode I/Mode II failure across all configurations. Overall, the results confirm that hybrid continuous-fiber-reinforced FDM composites can be systematically tailored through controlled layup design, providing a practical framework for optimizing additively manufactured structures.

ACKNOWLEDGEMENTS

The research was performed at Perm National Research Polytechnic University, with the support of the Russian Science Foundation (project no. 22-79-10350-P).

REFERENCES

[1] Cano-Vicent, A., Tambuwala, M.M., Hassan, S.S., Barh, D., Aljabali, A.A.A., Birkett, M., Arjunan, A., Serrano-Aroca, Á. (2021). Fused deposition modelling: Current status, methodology, applications and future prospects, Addit. Manuf., 47(September), p. 102378. DOI: https://doi.org/10.1016/j.addma.2021.102378.

[2] Penumakala, P.K., Santo, J., Thomas, A. (2020). A critical review on the fused deposition modeling of thermoplastic polymer composites, Compos. Part B Eng., 201(August), p. 108336. DOI: https://doi.org/10.1016/j.compositesb.2020.108336.

[3] Jiang, D., Smith, D.E. (2017). Anisotropic mechanical properties of oriented carbon fiber filled polymer composites produced with fused filament fabrication, Addit. Manuf., 18, pp. 84–94. DOI: https://doi.org/10.1016/j.addma.2017.08.006.

[4] Pepeliaev, A., Lobov, E., Vindokurov, I., Tashkinov, M. (2024). Comparison of mechanical properties of 3D-printed ABS, PA12 and PET-G reinforced with short fiber, Procedia Struct. Integr., 61(2023), pp. 224–231. DOI: https://doi.org/10.1016/j.prostr.2024.06.029.

[5] van de Werken, N., Tekinalp, H., Khanbolouki, P., Ozcan, S., Williams, A., Tehrani, M. (2020). Additively manufactured carbon fiber-reinforced composites: State of the art and perspective, Addit. Manuf., 31(November 2019), p. 100962. DOI: https://doi.org/10.1016/j.addma.2019.100962.

[6] Lobov, E., Dobrydneva, A., Vindokurov, I., Tashkinov, M. (2023). Effect of Short Carbon Fiber Reinforcement on Mechanical Properties of 3D-Printed Acrylonitrile Butadiene Styrene, Polymers (Basel)., 15(9), p. 2011. DOI: https://doi.org/10.3390/polym15092011.

[7] Lobov, E., Vindokurov, I., Tashkinov, M. (2024). Mechanical Properties and Performance of 3D-Printed Acrylonitrile Butadiene Styrene Reinforced with Carbon, Glass and Basalt Short Fibers, Polymers (Basel)., 16(8), p. 1106. DOI: https://doi.org/10.3390/polym16081106.

[8] Fu, Y.-T.T., Li, J., Guo, F.-L.L., Li, Y.-Q.Q., Fu, S.-Y.Y. (2024). Systematical mechanical analyses of 3D printed short carbon fiber reinforced polyetheretherketone composites, Compos. Part A Appl. Sci. Manuf., 185(August 2023), p. 108328. DOI: https://doi.org/10.1016/j.compositesa.2024.108328.

[9] Kabir, S.M.F., Mathur, K., Seyam, A.F.M. (2020). A critical review on 3D printed continuous fiber-reinforced composites: History, mechanism, materials and properties, Compos. Struct., 232(June 2019), p. 111476. DOI: https://doi.org/10.1016/j.compstruct.2019.111476.

[10] Park, G., Cho, N.-K., Lee, Y., Kim, C.-S. (2024). Comprehensive parametric analyses on the mechanical performance of 3D printed continuous carbon fibre reinforced plastic, Compos. Struct., 329(August 2023), p. 117804. DOI: https://doi.org/10.1016/j.compstruct.2023.117804.

[11] Wickramasinghe, S., Do, T., Tran, P. (2020). FDM-Based 3D Printing of Polymer and Associated Composite: A Review on Mechanical Properties, Defects and Treatments, Polymers (Basel)., 12(7), p. 1529. DOI: https://doi.org/10.3390/polym12071529.

[12] Heidari-Rarani, M., Rafiee-Afarani, M., Zahedi, A.M. (2019). Mechanical characterization of FDM 3D printing of continuous carbon fiber reinforced PLA composites, Compos. Part B Eng., 175(June), p. 107147. DOI: https://doi.org/10.1016/j.compositesb.2019.107147.

[13] Liu, F., Ferraris, E., Ivens, J. (2022). Mechanical investigation and microstructure performance of a two-matrix continuous carbon fibre composite fabricated by 3D printing, J. Manuf. Process., 79(November 2021), pp. 383–393. DOI: https://doi.org/10.1016/j.jmapro.2022.04.050.

[14] Li, S., Cheng, P., Ahzi, S., Peng, Y., Wang, K., Chinesta, F., Correia, J.P.M. (2023). Advances in hybrid fibers reinforced polymer-based composites prepared by FDM: A review on mechanical properties and prospects, Compos. Commun., 40(January). DOI: https://doi.org/10.1016/j.coco.2023.101592.

[15] Kong, X., Sun, G., Luo, Q., Brykin, V., Qian, J. (2024). Experimental and theoretical studies on 3D printed short and continuous carbon fiber hybrid reinforced composites, Thin-Walled Struct., 205, p. 112406.

DOI: https://doi.org/10.1016/j.tws.2024.112406.
[16] Chen, Y., Wei, X., Mao, J., Zhao, M., Liu, G. (2024). Experimental analysis of 3D printed continuous carbon/glass hybrid fiber reinforced PLA composites: Revealing synergistic mechanical properties and failure mechanisms, Polym. Compos., 45(12), pp. 10888–10897. DOI: https://doi.org/10.1002/pc.28516.
[17] Fernandes, R.R., Tamijani, A.Y., Al-Haik, M. (2021). Mechanical characterization of additively manufactured fiber-reinforced composites, Aerosp. Sci. Technol., 113, p. 106653. DOI: https://doi.org/10.1016/j.ast.2021.106653.
[18] Yavas, D., Zhang, Z., Liu, Q., Wu, D. (2021). Interlaminar shear behavior of continuous and short carbon fiber reinforced polymer composites fabricated by additive manufacturing, Compos. Part B Eng., 204(September 2020), p. 108460. DOI: https://doi.org/10.1016/j.compositesb.2020.108460.
[19] Xu, J., Yu, Y., Jia, X., Han, X., Akhmet, G., Yang, X. (2025). Experimental and Numerical Investigation of Tensile Performance in 3D-Printed Continuous Fiber-Reinforced Composites With Various Printing Paths and Materials Combinations, Polym. Compos., pp. 1–15. DOI: https://doi.org/10.1002/pc.70678.
[20] Dickson, A.N., Barry, J.N., McDonnell, K.A., Dowling, D.P. (2017). Fabrication of continuous carbon, glass and Kevlar fibre reinforced polymer composites using additive manufacturing, Addit. Manuf., 16, pp. 146–152. DOI: https://doi.org/10.1016/j.addma.2017.06.004.
[21] Shiratori, H., Todoroki, A., Ueda, M., Matsuzaki, R., Hirano, Y. (2021). Compressive strength degradation of the curved sections of 3D-printed continuous carbon fiber composite, Compos. Part A Appl. Sci. Manuf., 142(November 2020), p. 106244. DOI: https://doi.org/10.1016/j.compositesa.2020.106244.
[22] van de Werken, N., Hurley, J., Khanbolouki, P., Sarvestani, A.N., Tamijani, A.Y., Tehrani, M. (2019). Design considerations and modeling of fiber reinforced 3D printed parts, Compos. Part B Eng., 160(December 2018), pp. 684–692. DOI: https://doi.org/10.1016/j.compositesb.2018.12.094.